Morphology, Reversible Phase Crystallization, and Thermal Sensitive Shape Memory Effect of Cellulose Whisker/SMPU Nano-Composites

Jianping Han,[1] Yong Zhu,[1] Jinlian Hu,[1] Hongsheng Luo,[1] Lap-Yan Yeung,[1] Wenguo Li,[1] Qinghao Meng,[1] Guangdou Ye,[2] Sheng Zhang,[2] Ying Fan[2]

[1]*Institute of Textiles and Clothing, Hong Kong Polytechnic University, Kowloon, Hong Kong, People's Republic of China*
[2]*State Key Laboratory of Polymer Materials Engineering, Sichuan University, Chengdu 610065, China*

Received 26 April 2010; accepted 2 March 2011
DOI 10.1002/app.34505
Published online 8 August 2011 in Wiley Online Library (wileyonlinelibrary.com).

ABSTRACT: To investigate the morphology, crystallization properties of reversible phase and thermal sensitive shape memory properties of CW/SMPU (Cellulose Whisker/Shape Memory Polyurethane) nano-composite, the CW/SMPU nano-composite having CW contents of 0.1–3.8 wt % were prepared. SEM investigation showed the evolution of reversible phase morphology from spherolite crystallization structure to uniform matrix with tiny CW aggregates with the addition of CW into the SMPU matrix. DSC and isothermal crystallization kinetic method revealed the effect of CW on crystallization properties of reversible phase and fixed phase, suggesting that the effect of CW on the crystallization of hard segment phase is not comparable with thermal history; the more CW causes the higher crystallization rate of reversible phase; the crystallization mechanism of reversible phase in nano-composite gradually evolves to heterogeneous nucleation and crystal growth in two dimensions with the increase of CW content; the excellent nucleation effect of CW for the reversible phase leads to the drop of activity energy from 134.1 kJ/mol (*N*-0), to 95.1 kJ/mol (*N*-4). Cyclic tensile tests illustrate the addition of CW content can engender rapid shape fixity ability after a relative short cooling time; the shape fixity ratio of nano-composite and the control sample after sufficient cooling all can be identically high.
 J Appl Polym Sci 123: 749–762, 2012

Key words: nanocomposite; block copolymers; whiskers; crystallization; shape memory

INTRODUCTON AND OVERVIEW

Segmented shape memory polyurethanes, in which the soft segments comprise the reversible phase while the hard segments form the frozen phase, can restore its original shape upon heating above certain temperature, T_m (melting point) or T_g (glass transition) of soft segment after being strained. This unique feature of this type of material has aroused serious research interests from both academia and industry in recent two decades.[1–19] In the study of relations between the shape memory effect and molecular structure of segmented polyurethanes with poly(caprolactone)diols as the soft segment,[3,20,21] it was found that high crystallinity of the soft segment regions at room sdtemperature is a necessary prerequisite for shape memory function. In our previous research, SMPU ionomers were systematically studied and the results revealed that the disrupted physical crosslinks in hard segments can give rise to the rapid shape fixity, simultaneously illustrating the shape fixity ratio increases with the extension of cooling time,[22,23] suggesting the gradual increase of crystallinity during cooling time can favor the shape fixity ratio. Therefore, it is supposed that the rapid crystallization of soft segment potentially improves the shape fixity to temporary deformation in a short cooling time. Therefore, it is worth deepening the understanding about the crystallization properties for such smart materials.

Cellulose is one of the most abundant and renewable biopolymers from nature and has been studied broadly in both academic and industrial areas. The advantages of cellulose include low cost, low density, high stiffness, renewable nature, and biodegradability.[24] Enormous research has focused on the

Additional Supporting Information may be found in the online version of this article.

Correspondence to: J.L. Hu (tchujl@inet.polyu.edu.hk).

Contract grant sponsor: Hong Kong ITF research project; contract grant numbers: GHS/088/04, GHP/045/07TP.
Contract grant sponsor: Niche Area Fund of Hong Kong Polytechnic University; contract grant number: J-BB6*M*.
Contract grant sponsor: Opening Project of State Key Laboratory of Polymer Materials Engineering (Sichuan University); 200803.
Contract grant sponsor: the Hong Kong Research Grants Council project; contract grant number: RGC-GRF/518209.

composites reinforced with cellulose fiber. As for microcrystalline cellulose, in structure, cellulose chains aggregate to form micro-fibrils, long thread-like bundles of molecules stabilized laterally by hydrogen bonding between hydroxyl groups and oxygens of adjacent molecules. The arrangement of cellulose molecular chain in micro-fibrils is sufficiently regular to form monocrystalline cellulose domains. There is also an amount of cellulose in amorphous state within the micro-fibril.[25] Because of the different original resource, including the plants and some sea animals,[26] the cellulose micro-fibrils possess diameters ranging from 2 to 20 nm and the lengths that can be several tens of microns. The micro-fibril is a string of cellulose whiskers, assembled by the amorphous domains. The modulus of micro-fibrils can be close to the perfect crystal of native cellulose (estimated to 150 GPa). The amorphous domains as the defect can be removed from the micro-fibrils, so as to obtain the short microcrystals, i.e., cellulose whiskers. Dong et al. revealed that the hydrolysis condition, such as temperature and time, together with the subsequent ultrasonic treatment can be used to prepare the cellulose microcrystallites.[27] The length of prepared cellulose microcrystallites can be 75–107 nm evaluated from TEM images. Helbert et al. obtained the cellulose microcrystals with dimensions of $\sim$ 5 nm $\times$ 150–300 nm from wheat straw through a steam explosion method.[25] Oksman et al. established a technique quite suitable for industrial scale production, in which the partly separated cellulose nano-whiskers were observed after blending and extruding microcrystalline cellulose (MCC) with DMAc (*N*,*N*-Dimethyl acetamide)/LiCl (lithium chloride), PLA (polylactic acid), and PEG (polyethylene glycol) through extrusion at 170–200°C.[28] The results of Oksman shown the size of partly separated cellulose nano whiskers was approximately 10 nm in width and 200–400 nm in length, after suitable chemical and mechanical treatment. As for the nano-composite containing nano whisker with polymers as matrix, a series of studies were conducted. The high aspect ratio, modulus and strength of nano whiskers have urge researchers to deepen their studies to reveal the excellent reinforcement effect and other relevant advantages of this filler in nano scale[24,25,29] Moreover, it is quite interesting that the nano-composite containing rubber ethylene oxide-epichlorohydrin copolymer and whiskers from tunicates (the aspect ratio is higher than those from other sources) possess the architecture and mechanical adaptability closely similar to sea cucumber, which can selectively and reversibly be controlled through the formation and decoupling of a three dimensional network of well individualized nano fibers in response to specific chemical triggers.[30] Materials based on a rubbery host polymer and rigid whiskers shown a reversible change of tensile modulus by a factor of 40, with the stimulus of external chemicals that mediate the interaction among whiskers. Therefore, it can be seen the application of cellulose whiskers have been broadened from simple reinforcement to the smart or stimulus responsive materials.

In our study, taking account of the huge influence of the crystallizable reversible phase on the shape memory performance aforementioned, the first step is to elucidate the effect of cellulose whiskers within shape memory polymer matrix on the crystallization of soft segment phase i.e., reversible phase. To access the effectiveness of the shape memory function in practice, the copolymers are subjected to a testing routine including heating, deforming, and cooling of the sample. The testing cycle calls for a throughout understanding not only on the crystallinity, melting temperature of crystallization, but also on the crystallization rate and crystallizability. In this paper, the effect of CW loadings on the crystallizability and melting behavior were studied with isothermal crystallization kinetics. Two parameters in the Avrami theory, n and K, depending on the nucleation and crystal growth were determined. What's more, the crystallization rate and the activity energy of crystallization were discussed. For the nano-composites, the fracture surface after breaking in liquid nitrogen was observed. The WAXD was used to analyze the crystalline type of the reversible phase. In addition, cyclic tensile tests were used to compare the shape memory performance of CW/SMPU nano-composite with the control sample, to illustrate the influence of CW on the shape fixity and recovery ability.

EXPERIMENTAL

Sample preparation

The synthesis of SMPU composed of polycaprolactone diols (PCL), 4,4′-diphenylmethane diisocyanate (MDI) and 1, 4-butanediol (BDO) was detailed in supporting materials and one of our papers.[22] The soft segment was PCL with the molecular weight of 10,000. The hard segment content, simply counting MDI and BDO in, was 30 wt %. The cellulose whiskers were prepared from microcrystalline cellulose(MCC) (Cellulose, microcrystalline, colloidal, CAS 51395-75-6, Aldrich, USA) by hydrolysis treatment (64 wt % sulfuric acid in water for 1 h at 50°C). The condition for hydrolysis was selected according to the previous literature.[27,31] Subsequently, the suspension was washed with centrifuge and water until acid free. Then the cellulose whiskers dehydrated from the suspension by freeze-drying were dispersed in Dimethylformamide

TABLE I
The Composition of the Control Sample, Cellulose Whisker/SMPU Composites, Microcrystalline Cellulose/ SMPU Composites

Samples	Wisker content (wt%)	Samples	Microcrystal cellulose content (wt %)
N-0	0%	NC-3	2.88%
N-0.1	0.10%	NC-5	5.51%
N-0.25	0.25%		
N-1	1.03%		
N-2	1.97%		
N-4	3.81%		

(DMF) in the concentration of 0.5 wt % to prepare the homogeneous suspension by vigorous mixing and ultrasonic vibrations (BRANSONIC-2510E-MT, 100 w, 40 kHz, Branson Ultrasonic Corp., USA). CW/SMPU nano-composite were prepared by mixing the CW suspension with SMPU in DMF for one day in 5 wt % solid content. Then the films were prepared by transferring the CW/SMPU suspension to Teflon molds and allowed them to solidify at 60°C in air for 24 h. To remove the residual DMF, the films were held at 75°C under vacuum of 1–2 mmHg for 24 h. The nominal thickness of the films was about 200 μm. The preparation condition for all samples was the same to make sure the thermal history of prepared samples was identical. As shown in Table I, the series of nano-composite are nomenclated by the letter "N" and followed by the numbers showing the approximate loading content. The untreated MCC was dispersed in DMF with 5 wt %, and then mixed with SMPU to prepare the dispersion, and finally make film samples in the aforementioned way. The samples with MCC as fillers are denoted with "NC-3" and "NC-5."

Characterization

Isothermal crystallization experiments were performed using a Perkin–Elmer Diamond DSC. The heating and cooling routine, isothermal crystallization temperature was set to the quite similar to that used in shape memory function investigation.[32] All the detection was purged with nitrogen gas and cooled by a cooler (Perkin–Elmer, Intracooler II). Indium and zinc standards were used for calibration. The sample (~ 4–6 mg) was initially heated to 75°C at a rate of 10°C/min and held at 75°C for 5 min to remove the thermal history of the crystallizable phase, then rapidly (60°C/min) cooled to a designated crystallization temperature T_c, and held at this temperature to the end of the exothermic crystallization. The heat of fusion during the isothermal crystallization process was recorded as a function of time. The T_c was chosen in practical ranging from 16 to 32°C. The amounts of heat generated during the development of crystal phase were recorded and analyzed according to the usual equation of evaluating the relative degree of crystallinity X_t:

$$X_t = \frac{\int_{t_0}^{t} (\frac{dH}{dt})dt}{\int_{t_0}^{t=\infty} (\frac{dH}{dt})dt} \quad (1)$$

where t_0 and $t = \infty$ are the time at which the sample reached isothermal conditions (as indicated by a flat base line after an initial spike in the thermal curve) and the time at which the dominant sharp exothermic peak ended. H is the enthalpy of crystallization at time t. After isothermal crystallization, the sample was heated to 75°C and the melting temperature T_m indicated by the maximum of the endothermic peak was recorded.

An instrument of Transmission Electron Microscopy (TEM, JEOL-2010 with the accelerate voltage of 200 kV) was applied to observe cellulose whiskers dispersed in DMF suspension. Ultrasonic treatment was conducted to individualize the cellulose whiskers and the dimensional estimation was made according to the TEM images. The dilute suspension containing cellulose whiskers with DMF as solvent was dropped onto the carbon film on the copper grid. Thereafter the sample grids are dried sufficiently in air for TEM observation. A JEOL JSM-6490 Scanning Electronic Microscopy (SEM) instrument was used to investigate the morphology of the fracture surface of film samples after freezing in liquid nitrogen. The surface observed was coated with gold on JEOL JFC-1100E ion sputter coater in advance. The SEM micrographs were obtained by using 7 kV secondary electrons. The nano-composites and original MCC were investigated with thermogravimetric analysis (Netzsch STA449C) from room temperature up to the decomposed temperature with the Argon as purge gas, so as to detect the thermal stability of specimens. The heating rate was 10°C/min in the range of room temperature to 550°C. The thermal properties were investigated by Differential Scanning Calorimetry (DSC, Perkin–Elmer Diamond), purged with nitrogen gas and cooled by a cooler (Perkin–Elmer, Intracooler II). Indium and zinc standards were used for calibration. To ensure a consistent thermal history for the melting process, the samples were heated to 220°C and kept for 3 min. After that they were cooled to −40°C at a cooling rate of 20°C/min, and then heated to 220°C at a rate of 20°C/min and the thermograms were recorded and compared. Wide Angle X-ray Diffraction (WAXD) profiles of prepared samples were measured with Philip Xpert XRD System by Nickel-filtered CuKa radiation (wave length = 0.1542 nm) at operating voltage of 40 kV and a current of

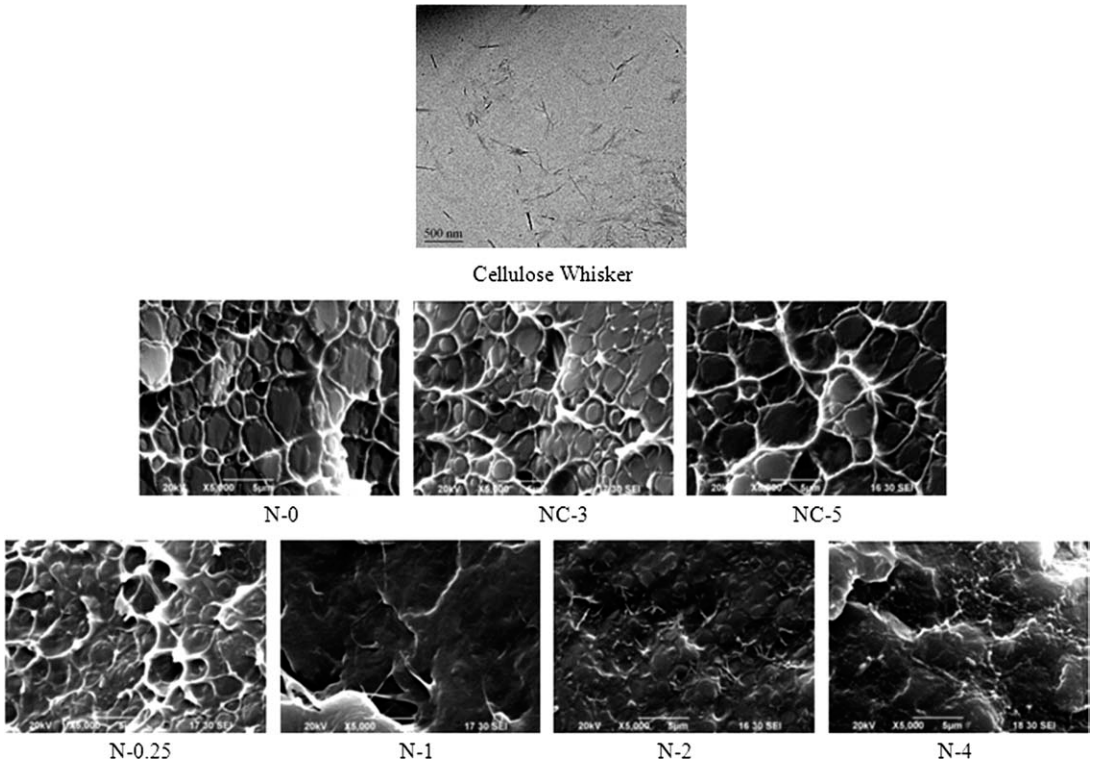

Figure 1 TEM image of cellulose whisker from MCC treated by hydrolysis (upper); SEM images of control sample (*N*-0), MCC/SMP composites (NC-3 and NC-5), and CW/SMP nano-composites (lower).

30mA. The scattering intensity was recorded in the range of 10–40° with the goniometer arm speed of 0.03°/s.

The cyclic tensile test was performed using an INSTRON 5566 universal tensile tester equipped with a temperature control chamber. The standardized film size was 5 × 20 mm^2. The film was heated initially to 75°C (T_{high}) in 600 s. After the sample was stretched to 50% or 100% elongation (ε_m) at T_{high} with a stretching rate of 10 mm/min, cool air was vented passively into the chamber to quench down the sample to around 24°C (T_{low}) at ε_m during various cooling time (15, 30, 300 s). Then, the strain was released from ε_m to 0 and the recurrent heating and cooling process start subsequently. The complete thermal cycle for each sample was repeated five times for assessing the shape memory effect. Detailed parameter definitions such as shape recovery ratio (R_r) or shape fixity ratio (R_f) used to characterize the shape memory effect were defined in literature.[9,14,15] Thereof, R_r quantifies the ability of the materials to memorize its permanent shape and is defined as the strain recovery after several passed cycles based on the original shape of the sample (eq. 9); R_f is given by the ratio of the strain in the stress-free state after the retraction of the tensile stress in one of cycles and the maximum strain (eq. 10). The specific calculation was detailed in the part of discussion.

RESULTS AND DISCUSSION

Figure 1 (upper graph) from TEM illustrate that cellulose whiskers obtained from the hydrolysis treatment presenting the relative uniform distribution in nano scale. The diameter of prepared cellulose whiskers is about 20–30 nm and the length is 200–500 nm. Therefore, the aspect ratio of CW estimated from TEM is about 10∼, which is consistent with other researchers' result.[25,33] The dimension of prepared CW not only depends on the hydrolysis condition,[27] but also bases on the raw source such as 20 nm for Valonia, 10 nm for tunicin, 5 nm for ramie, 3–4 nm for wood and 1.5–3.0 nm for bacterial cellulose.[25] SEM was used to characterize the morphology of CW/SMPU nano-composite. The comparison among the control sample without fillers, MCC/SMPU composites, and CW/SMPU nano-composites were made to study the influence of cellulose whiskers on SMPU matrix. As shown in Figure 1 (lower graph), the spherolite crystal structures with the diameter of 2-5 μm was observed in *N*-0, NC-3, and NC-5. In *N*-0.25, the shperolite structures are becoming blurred. When the loading content of CW increases from 0.25 (*N*-0.25) to 1.03 (*N*-1), 1.97 (*N*-2) and 3.81 wt % (*N*-4), the morphology of fracture surfaces evolves from obvious spherolites to uniform matrix with tiny CW aggregates. It can be explained that CW aggregates appear as white stains in the

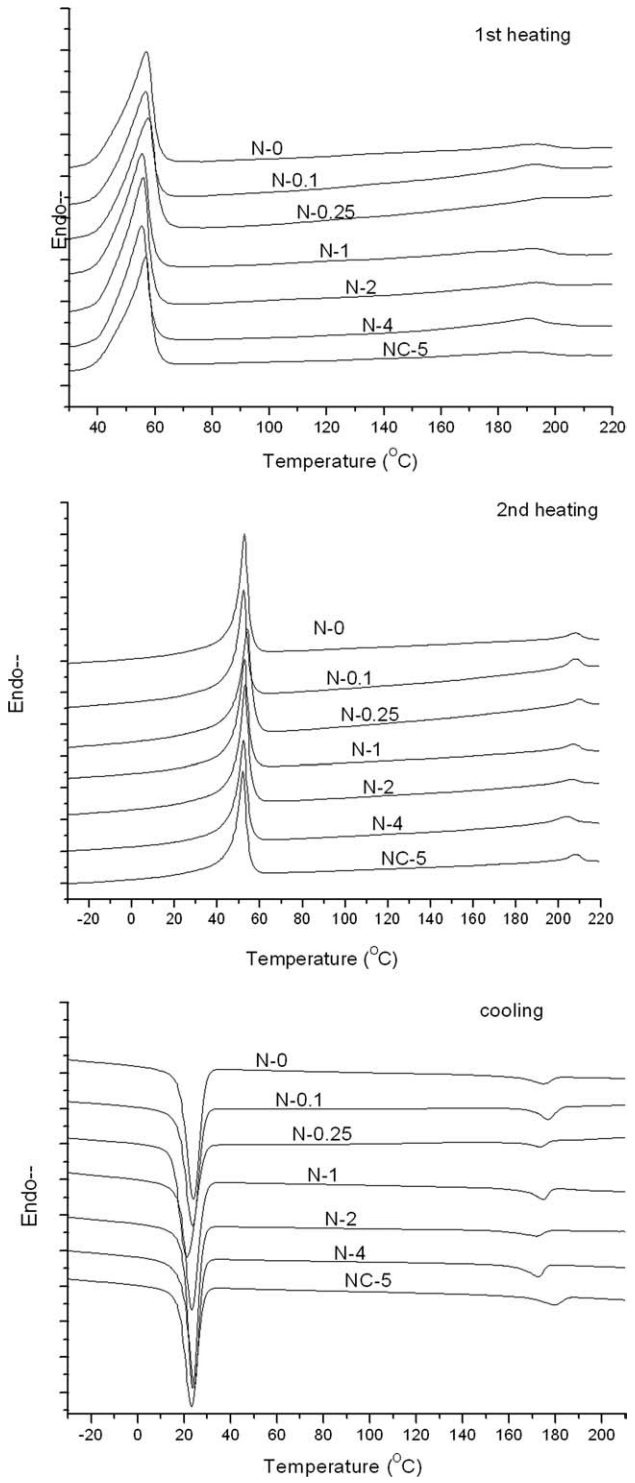

Figure 2 Heating and cooling scan for *N*-0, NC-5, and CW/SMPU nano-composites through DSC.

fracture surface and are roughly dispersed within the polymeric matrix, to form filler domains surrounded by the synthetic matrix.[25] On the other hand, due to the nucleation effect of CW dispersion, the dimension of spherolite crystal of reversible phase of SMPU probably decreases. The average size of spherolites or the nucleation density is dependant on the rates of nucleation and the following growth of the spherolites. If the nucleation is faster, then the spherolites formed after the impingement of micro crystallites would be thought to be smaller.[34] It might be the reason of the disappearance of shperolite structure in CW/SMPU nano-composites. The thermal stability was studied through TGA. Figure S2 (in Supportin Information) illustrating that the small addition of CW in the SMPU matrix can improve the thermal stability of the nano-composite. Especially, the 1.97 and 3.81 wt % (*N*-2 and *N*-4) CW improve the decomposition temperature of 80% weight loss upward to the high temperature. Instead, the pure MCC and pure SMPU (*N*-0) present the worse thermal stability in comparison with nano-composite series and NC-5. In DSC heating scan, the thermograms of all samples studied show the endothermic melting peak of soft segment phase and hard segment phase when heated as shown in Figure 2. The data about thermal properties are summarized in Table II. Obviously, from the two melting peaks located at 51–57°C and 188–209°C shown in heating scans of Figure 2, it can be found there are two-phase structures. One is crystalline soft segment phase and the other one belongs to hard segment phase with weak crystallization endothermic peak. Brunette and coworkers ever studied the model hard segment compound, BDO-MDI with DSC and FTIR to reveal the temperature dependence of hydrogen bonding, and concluded that the sufficient annealing at 150°C can effectively convert the non-crystalline domain structure to the crystalline state, which give rise to the well-defined high temperature transition at 200–230°C.[35] Therefore, it can be found the crystallization of hard segment phase is quite related to the thermal history and particular composition. In our study, in the 2nd heating scan, the relatively well defined melting peak of hard segment phase can be detected for *N*-0, NC-5, and all CW/SMPU nano-composites. In the 1st heating, the melting peak of hard segment phase is almost neglectable, except for the tiny melting peak located around 190°C. It is concluded that the effect of fillers in this series of samples on the crystallization of hard segment phase is not comparable to thermal history. On the other hand, for the soft segment phase, the melting enthalpy in the 2nd heating scan of all composites is slightly lower than *N*-0. But it is not sufficient for evaluating the crystallizability of all samples to give an explanation to the morphology evolution. So, in the following part, isothermal crystallization kinetic was applied to detail crystallization properties of soft segment phase.

The heating-cooling routine in isothermal crystallization was set to the similar to that for shape memory programming reported previously.[22,32] The

TABLE II
Thermal Properties Detected by DSC

	1st heating scan				Cooling scan				2nd heating scan			
Sample	T_{ms} (C°)	ΔH_{ms} (J/g)	T_{mh} (C°)	ΔH_{mh} (J/g)	T_{cs} (C°)	ΔH_{cs} (J/g)	T_{ch} (C°)	ΔH_{ch} (J/g)	T_{ms} (C°)	ΔH_{ms} (J/g)	T_{mh} (C°)	ΔH_{mh} (J/g)
N-0	56.8	45.9	193.8	–	23.9	38.3	174.6	2.76	52.6	43.0	207.8	2.68
N-0.1	56.8	43.6	192.5	–	23.5	37.9	176.6	4.55	52.3	38.8	207.8	3.40
N-0.25	57.8	48.2	196.2	–	20.9	42.2	173.3	2.16	54.0	42.2	209.8	1.93
N-1	55.4	43.6	193.2	–	23.2	40.4	174.6	3.71	52.6	40.5	199.3	2.68
N-2	55.7	47.0	192.8	–	23.6	41.2	171.6	2.49	52.9	42.5	206.1	2.33
N-4	55.4	42.2	190.5	–	24.2	36.3	172.6	4.50	52.3	37.3	203.8	3.78
NC-5	56.8	40.7	188.2	–	22.9	36.5	179.6	3.63	51.9	36.5	208.1	2.42

T_{ms}, melting temperature of soft-segment; ΔH_{ms}, enthalpy of melting soft-segment; T_{mh}, melting temperature of hard-segment; ΔH_{mh}, enthalpy of melting hard-segment; T_{cs}: temperature of soft-segment crystallization; ΔH_{cs}, heat of soft-segment crystallization; T_{ch}, temperature of hard-segment crystallization; ΔH_{ch}, heat of hard-segment crystallization.

overall kinetics of the isothermal crystallization of crystalline soft segment from the melt is analyzed on the basis of the Avrami equation.[36] This crystallization theory is widely accepted to describe the crystallization process in polymer, polymer blends, and copolymers.[37–42] The Avrami equation is used to describe the crystallization kinetics:

$$X(t) = 1 - \exp(-Kt^n) \tag{2}$$

which can be linearized in the form:

$$\log[-\ln(1 - X(t))] = n \log t + \log K \tag{3}$$

where n is the Avrami exponent whose value depends upon the mechanism of nucleation and on the crystal-growth geometry, K is a rate constant containing the nucleation and the growth parameters. $X(t)$ represents the relative amount of crystallization plotted in Figure 3 for different crystallization temperatures and in Figure 4 for CW/SMPU nanocomposites with various loading content of CW at 32°C. Therefore, if the crystallization rate can be compared according to the time to finish the isothermal crystallization, it can be observed that the higher the isothermal crystallization temperature, the lower the crystallization rate will be; the crystallization rate increases with the increase of CW content. Especially in *N*-4, the isothermal crystallization can be finished in the shortest time among all samples, judging from the curve of heat generated versus time in Figure 4. Also, in the comparison between *N*-0 and NC-5, it can be observed that the crystallization rate can be increased slightly when original MCC was used as fillers, suggesting the MCC in the SMPU matrix also can present nucleation effect to speed up the crystallization of the soft segments. Theoretically, if eq. (3) can adequately follow the crystallization process, a plot of $\log[-\ln(1 - X(t))]$ against $\log t$ should yield a straight line with slope n and intercept $\log K$. The double logarithmic plots of $\log[-\ln(1 - X(t))]$ against $\log t$ with various temperatures are shown in Figure 5(a) (upper graph). Each plot represents a linear dependence of $\log[-\ln(1 - X(t))]$ against $\log t$, but of slightly deviation from the prediction when both parameters are large, indicating the existence of a secondary crystallization of PCL which occurs consecutively with primary. The study of PCL (M_w = 80,000) by Kuo et al.[43] suggests that the PCL with a higher M_w value has the same tendency at a later stage in the crystallization process. The deviation is attributed to the secondary crystallization involving fibrillar growth between the primary lamellae of the spherolite, and leading to the occurrence of spherolite impingement.

The values of n and K for a particular sample can be determined from the initial linear portions of the double logarithmic plots of Figure 5(a). The results for different samples are summarized in Table III, Figure 5(b,c). The Avrami parameter n of *N*-0 and NC-5 at 16–32°C in our investigation is around 2.5 and present the slight increasing trend with the increase of temperature. As shown in Figure 5(b), in nano-composites, when the CW loading ratio is increased from 0 to 3.81 wt %, the n value calculated from eq. (3) and Figure 5(a) decreases from around 2.5 to 1.5–2.0, suggesting CW has a substantial influence on the nucleation and crystal growth mechanism. Generally, the n value close to 3 may represent an athermal nucleation processing with three-dimensional crystal growth. The n value close to 2 means the crystal growth may not undergo in three dimensions at the equal rate. The integral n value obtained in this study might be caused by the crystalline branching or secondary crystallization. Therefore, it can be seen that the introduction of CW into SMPU matrix give rise to the enhancement of heterogeneous nucleation and crystal growth in two dimensions.

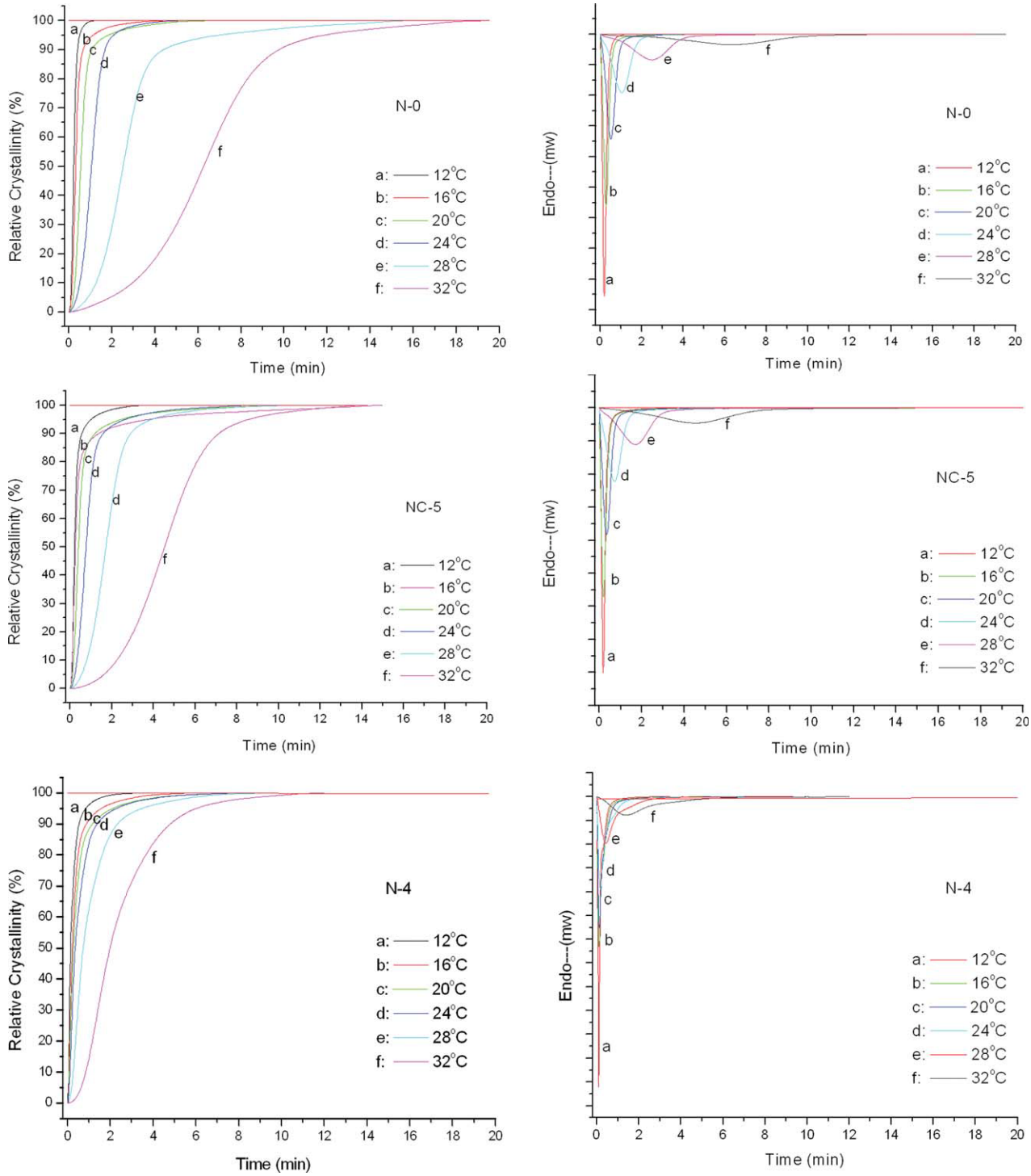

Figure 3 Relative crystallinity and exothermal heat versus time during isothermal crystallization at 12, 16, 20, 24, 28, 32°C. [Color figure can be viewed in the online issue, which is available at wileyonlinelibrary.com.]

The half crystallization time $t(0.5)$ is defined as the time at which the crystallinity is equal to 50%. In Avrami eq. (2), when $X(t) = 50\%$:

$$K = \ln 2/[t(0.5)]^n \tag{4}$$

In Table III, the half crystallization time $t(0.5)$ calculated from eq. (4) agrees with that obtained experimentally from Figure 3, suggesting that the Avrami equation analysis is adequate to describe the crystallization mechanism of the reversible phase in the series of SMPU and the nano-composite.[44] The rate of crystallization is mathematically defined as the inverse of $t(0.5)$. From Figure 5(c) it is found that the crystallization rate increases significantly with the increase of CW content. At the isothermal

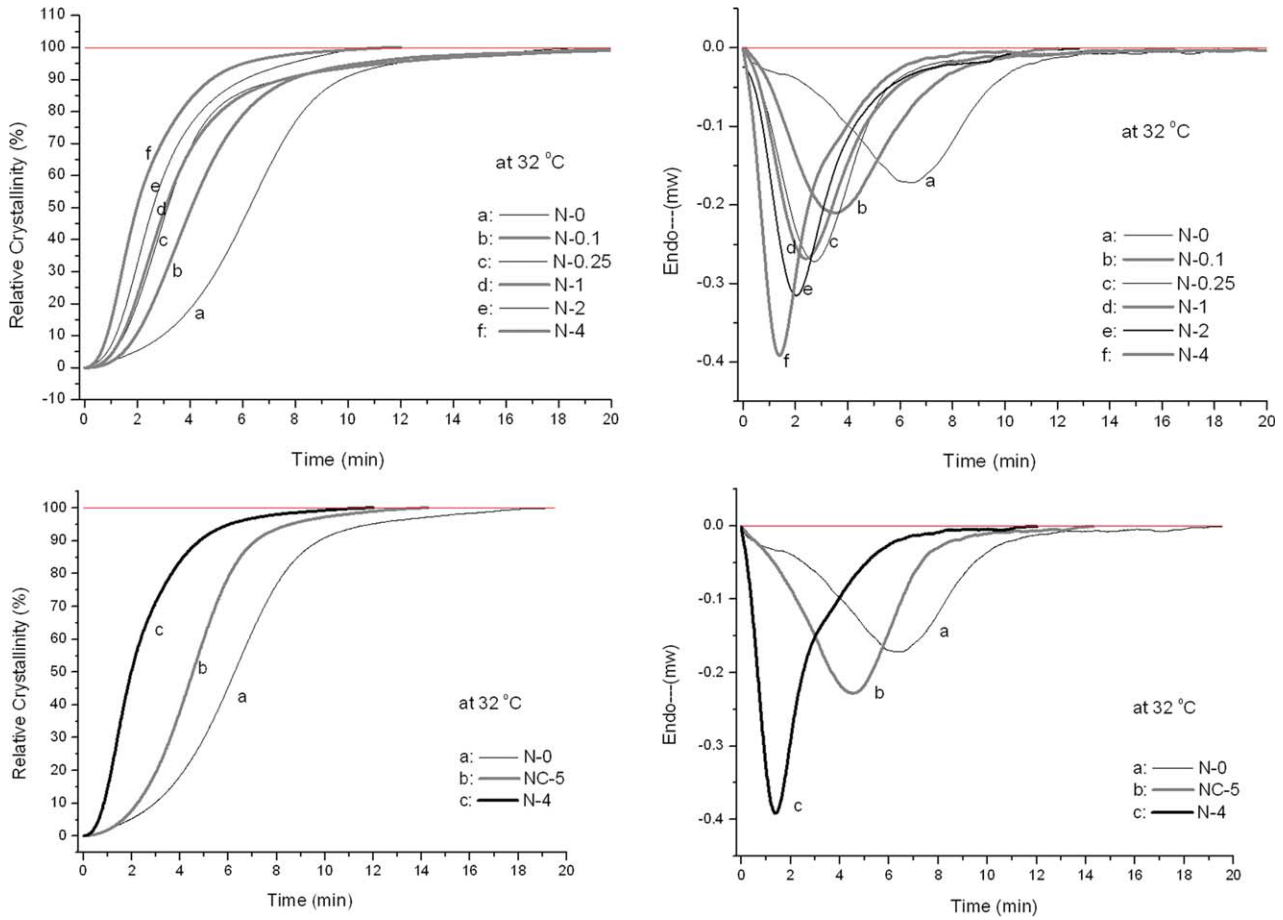

Figure 4 Relative crystallinity and exothermal heat during isothermal crystallization at 32°C. [Color figure can be viewed in the online issue, which is available at wileyonlinelibrary.com.]

crystallization temperature of 32°C, only 3.81 wt % CW can make the time of half crystallinity ($t(0.5)$) decrease from 6.26 min in pure SMPU to 1.98 min in *N*-4. While $t(0.5)$ in the sample NC-5 with the loading content of MCC of 5.51 wt % in SMPU matrix is 4.53 min.

As shown in heating scan after isothermal crystallization (detailed in Figure S1 in Supporting Information), a dominant sharp exothermic peak in the reheating DSC thermogram of our samples is considered to be the primary melting temperature (T_m). In Figure S3 (in Supporting Information), the T_m of all samples for various T_c is summarized in a figure and it clearly reveals that T_m increases linearly with T_c. The T_e can be calculated by linear extrapolation of T_m versus T_c to the line $T_m = T_c$ and listed in Table III. The experimental data can be fitted well by the Hoffman-Weeks equation[46]:

$$T_m = \Phi T_c + (1 - \Phi) T_e \tag{5}$$

where T_e is the equilibrium melting point, and $\Phi = 1/\gamma$ is the stability parameter depending on the crystal thickness (γ is the ratio of the lamellar thickness L to the lamellar thickness of the critical nucleus L^* at T_c). The Φ is between 0 and 1 ($\Phi = 0$ and $T_m = T_e$, whereas $\Phi = 1$ and $T_m = T_c$). The crystal are most stable for $\Phi = 0$ and unstable for $\Phi = 1$. As shown in Figure S3, T_m increases with T_c as expected. The extrapolation of the observed melting temperatures to the line $T_m = T_c$ has been employed to calculate the T_e of copolymers and homopolymers.[47] However, in the case of the study on segmented poly (ester-urethanes) based on poly(ε-caprolactone) by Bogdanow et al.,[48] linear polyethylene, and random copolymers at low level of crystallinity by Alamo et al.,[49,50] this extrapolation method fails to describe the relations between T_m and T_c. Firstly, the nonisothermal crystallization during cooling to certain T_c causes the corresponding T_m to increase. Secondly, the observed dependence also arises from annealing during the heating scan which causes the improvement in crystal quality and hence T_m increases, and the effect is particularly pronounced when T_c is lower. Therefore, in our investigation, T_e is calculated from the crystallization temperatures range

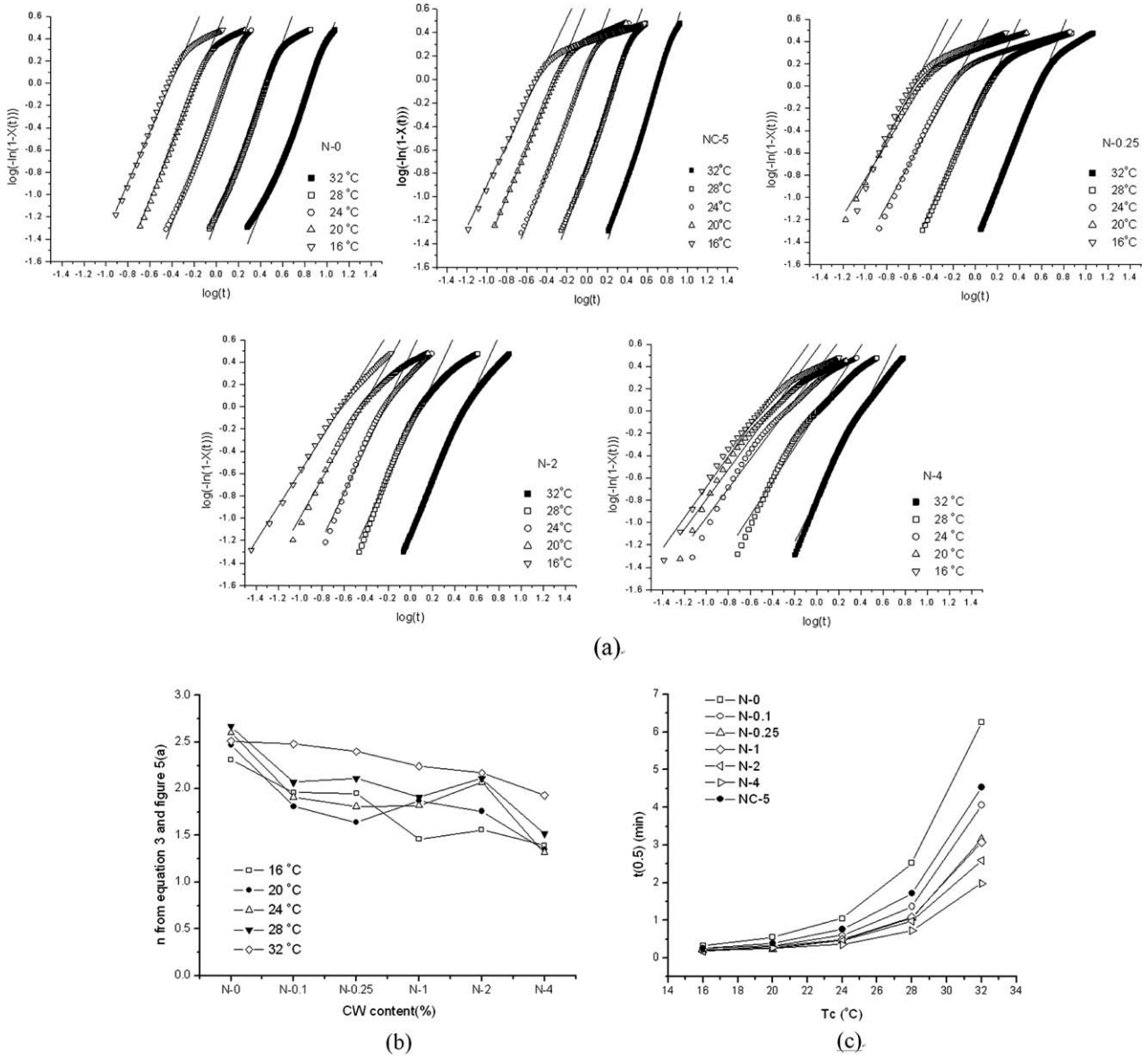

Figure 5 The double logarithmic plots of log[-ln(1-$X(t)$)] against logt (a) (upper); The evolution of n value (b) and the dependence of $t(0.5)$ on T_c (c).

above 24°C. Table III summarizes values of equilibrium melting temperature (T_e) of all samples. It is found that the T_e and Φ values of nano-composite are quite similar to *N*-0. In *N*-4, the stability parameter Φ varies from 0.20 to 0.23. It is slightly higher than *N*-0, 0.19–0.21, suggesting that the formation of crystals of reversible phase in CW/SMPU nano-composite is rather stable. In addition, from the XRD profiles shown in Figure 6 for pure MCC, *N*-0, *N*-2, *N*-4, NC-3, and NC-5, it is observed that the crystalline structure of the reversible phase in SMPU is not influenced significantly. The two intense reflection peaks appear at $2\theta = 22^\circ$ and 23.8°, illustrating the reversible phase in CW/SMPU nano-composite and pure SMPU are characteristic of the orthorhombic crystalline form. Pure MCC presents peaks at $2\theta = 15.4^\circ$, 16.2° and 22.5°, suggesting the crystalline structure in MCC belongs to cellulose I polymorph. The isothermal crystallization process in nano-composite is assumed to be thermally activated. The Avrami paprmeter K can then be described by the Arrhenius equation[37,42]:

$$K^{1/n} = k_o \exp\left(-\frac{\Delta E}{RT_c}\right) \tag{6}$$

$$(1/n)\ln K = \ln k_o - \frac{\Delta E}{RT_c} \tag{7}$$

where k_0 is a temperature-independent pre-exponential factor, R is the gas constant, and ΔE is the total

TABLE III
Parameters for Isothermal Crystallization

	T_c (C°)	n[a]	logK[a]	K[a]	$t(0.5)$[b]	$t(0.5)$[c]	T_m (C°)	ΔH[d] (J/g)	T_e (C°)	Φ[e]
N-0	16	2.31	0.95	9.00	0.329	0.317	49.36	35.90	57.38	0.194
	20	2.47	0.45	2.81	0.567	0.556	49.87	34.70		0.201
	24	2.60	−0.21	0.61	1.050	1.054	50.37	34.40		0.210
	28	2.67	−1.23	0.06	2.500	2.519	51.20	32.50		0.210
	32	2.51	−2.15	0.01	5.412	6.260	52.05	30.20		0.210
N-0.1	16	1.96	0.93	8.55	0.277	0.256	48.69	28.90	56.70	0.197
	20	1.81	0.66	4.59	0.352	0.329	49.20	28.10		0.204
	24	1.91	0.23	1.71	0.623	0.598	49.87	27.50		0.209
	28	2.07	−0.46	0.35	1.391	1.369	50.70	25.40		0.209
	32	2.48	−1.68	0.02	4.177	4.059	51.54	23.10		0.209
N-0.25	16	1.95	1.09	12.20	0.229	0.212	49.02	33.60	57.08	0.196
	20	1.64	0.80	6.32	0.260	0.243	49.35	32.70		0.208
	24	1.81	0.38	2.42	0.501	0.470	50.19	31.40		0.208
	28	2.11	−0.25	0.56	1.106	1.073	50.86	29.60		0.214
	32	2.40	−1.38	0.04	3.282	3.152	51.87	27.40		0.208
N-1	16	1.46	0.79	6.15	0.224	0.202	48.83	34.50	57.57	0.210
	20	1.87	0.72	5.21	0.340	0.308	49.16	33.50		0.224
	24	1.82	0.33	2.15	0.537	0.494	49.83	33.00		0.231
	28	1.91	−0.28	0.52	1.162	1.084	50.67	31.00		0.233
	32	2.24	−1.29	0.05	3.234	3.068	51.68	27.70		0.230
N-2	16	1.56	0.98	9.45	0.187	0.178	49.34	33.80	57.43	0.195
	20	1.76	0.76	5.81	0.298	0.276	49.67	33.20		0.207
	24	2.07	0.48	3.00	0.493	0.465	50.50	32.30		0.207
	28	2.11	−0.20	0.63	1.046	0.985	51.17	31.30		0.213
	32	2.17	−1.10	0.08	2.704	2.592	52.17	29.10		0.207
N-4	16	1.39	0.71	5.07	0.239	0.224	48.69	34.20	57.29	0.208
	20	1.35	0.56	3.60	0.295	0.268	49.02	33.10		0.222
	24	1.32	0.36	2.31	0.402	0.359	49.70	32.70		0.228
	28	1.52	−0.02	0.95	0.812	0.731	50.53	30.50		0.231
	32	1.93	−0.79	0.16	2.137	1.983	51.53	27.40		0.228
NC-5	16	1.79	0.88	7.58	0.262	0.249	49.00	33.50	57.06	0.196
	20	2.05	0.65	4.42	0.405	0.397	49.50	31.60		0.204
	24	2.22	0.10	1.27	0.761	0.760	50.17	30.70		0.208
	28	2.45	−0.73	0.18	1.733	1.718	50.85	28.80		0.214
	32	2.68	−1.92	0.01	4.862	4.533	51.85	26.30		0.208

[a] n and K value obtained from eq. (3) and Figure 5(a).
[b] t(0.5) calculated from eq. (4) using and n a and K a value.
[c] $t(0.5)$ obtained experimentally from Figure 3.
[d] Melting enthalpy in heating scan at 10C°/min after isothermal crystallization.
[e] Φ calculated from eq. (5).

crystallization activation energy in kJ/mol. The plots of $(1/n)\ln K$ against $1/T_c$ are shown in Figure S4 (in Supporting Material). The activation energy is calculated and summarized in Table IV. For N-0, the ΔE for the primary crystallization process is calculated to be 134.1 kJ/mol, while for N-2 and N-4, the ΔE decreases significantly to 117.8 and 95.1 kJ/mol. In the sample NC-5 containing MCC, the ΔE is 127.7 kJ/mol. The decrease trend of activation energy in nano-composites indicates that the effect of temperature on crystallization rate becomes smaller with the increase of CW content. In this isothermal crystallization, the nucleation is dominant. Therefore, it can conclude that nucleation mode exhibits the tendency to more athermal one. The addition of CW with the huge surface of unit mass is able to speed up the crystallization of the reversible phase. It is potentially used for the rapid shape fixity as bio-materials for immobilization or rehabilitation usage.[22]

Because the crystallization of the reversible phase is time-dependant, the cyclic tensile test routine with different cooling time was designed to investigate shape fixity to transient deformation. The parameters such as shape fixity ratio and shape recovery ratio for this testing have already been reported previously.[1,32] In cycle tensile testing, the stress–strain curves of the segmented polyurethane films tend to be identical after the first several cycles and with no significant variation in further cycles as reported before.[7,9,12,13,51] It is due to the destruction of weak net-points in the initial cycles in deformation, and the subsequent formation of ideal elastic network.[1]

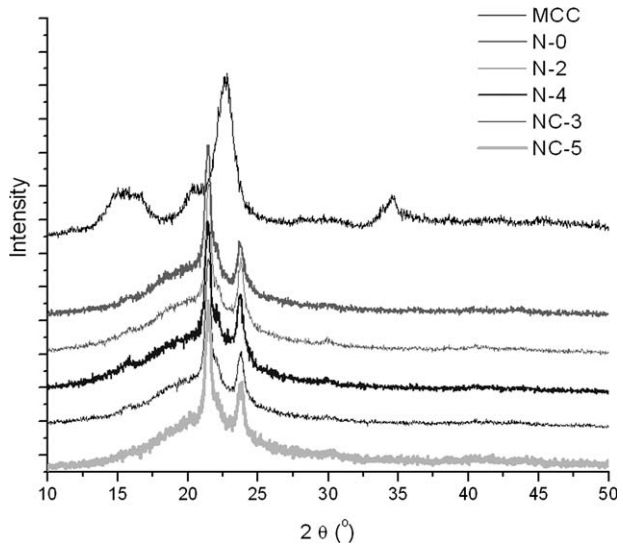

Figure 6 XRD profile for MCC and composites.

Therefore, the fixed strain (ε_u) and irreversible strain (ε_p) of cycle 2 to 5 are used to assess shape memory effect in this article.

$$R_r = \frac{\varepsilon_m - \varepsilon_p}{\varepsilon_m} \times 100\% \quad (8)$$

$$R_f = \frac{\varepsilon_u}{\varepsilon_m} \times 100\% \quad (9)$$

where ε_m represents the maximum strain in the cyclic tensile testing; ε_u is the residual strain after unloading at T_{low}; ε_p is the residual strain after shape recovery. In this study, R_f s and R_r s of cycle 2 to cycle 5 are averaged to demonstrate the effect of the composition on shape memory performance.

As the results reported previously, the shape fixity ratio increases gradually with the increase of cooling time.[22] Furthermore, it can be seen, from Table V, Figures 7 and 8, that the R_f of *N*-4 is much higher than that of *N*-0 when cooling time is relative short such as 15 s. But after sufficient cooling time such as 300 s, the R_f of *N*-4 is approximately identical to the control sample, *N*-0. For shape recovery ratio, the difference between the two samples is not significant in comparison to shape fixity performance. It can be explained that the addition of cellulose whiskers mostly influences the crystallization process of the reversible phase. Especially, when the cooling time is insufficient (15 s), the crystallization of reversible phase in *N*-4 can be formed more rapidly to withstand the internal stress stored in deformed polymer network. Therefore, shape fixity in *N*-4 for 15 s cooling time is much higher. After sufficient cooling time, all crystallization is formed very well in both *N*-4 and *N*-0. It should be the reason of the similar shape fixity ratio in the two samples for shape fixity with sufficient cooling (300 s).

TABLE IV
Crystallization Activation Energy from Figure 5(a) and eq. (4)

Sample code	ΔE (kJ/mol)[a]	ΔE(kJ/mol)[b]
N-0	134.1	136.2
N-0.1	121.8	125.1
N-1	116.3	119.1
N-2	117.8	118.3
N-4	95.1	94.6
NC-5	127.7	130.0

[a] Calculated by using *K* and *n* value from Figure 5(a).
[b] Calculated by using *K* and *n* value from eq. (4) where t(0.5) are experimentally from Figure 3.

CONCLUSIONS

The morphology, crystallization of reversible phase and shape memory performance of CW/SMPU nano-composites were investigated by using SEM, XRD, TGA, DSC, and cyclic tensile test. The spherolite crystal structures with the diameter of 2–5 μm can be observed in *N*-0, NC-3, and NC-5. But, for nano-composites, the facture surfaces evolves from obvious spherolites to uniform matrix with tiny cellulose whisker aggregates. The thermal stability of all composites is better than the pure SMPU and untreated microcrystal cellulose. Especially, the 1.97 and 3.81 wt % (*N*-2 and *N*-4) CW can improve the decomposition temperature of 80% weight loss upward to the high temperature. DSC heating thermogram of the two melting peaks located at 51–57°C(soft segment phase) and 188–209°C(hard

TABLE V
Shape Fixity and Shape Recovery Ratio of N-0 and N-4

	Cooling time (s)	15	15	30	300
Sample code	Maximum strain (mm/mm)	0.5	1	1	1
N-0	Rf (%)	55.05 ± 3.7	71.68 ± 2.0	82.6 ± 1.6	94.0 ± 0.4
	Rr (%)	86.18 ± 1.6	91.06 ± 1.2	89.63 ± 1.1	84.18 ± 1.6
N-4	Rf (%)	58.45 ± 0.8	76.55 ± 0.9	85.58 ± 1.4	94.77 ± 0.2
	Rr (%)	87.55 ± 1.2	88.28 ± 1.1	88.71 ± 1.1	87.15 ± 1.5

R_f and R_r values represent the average values (number of measurement is 4) ± standard deviation.

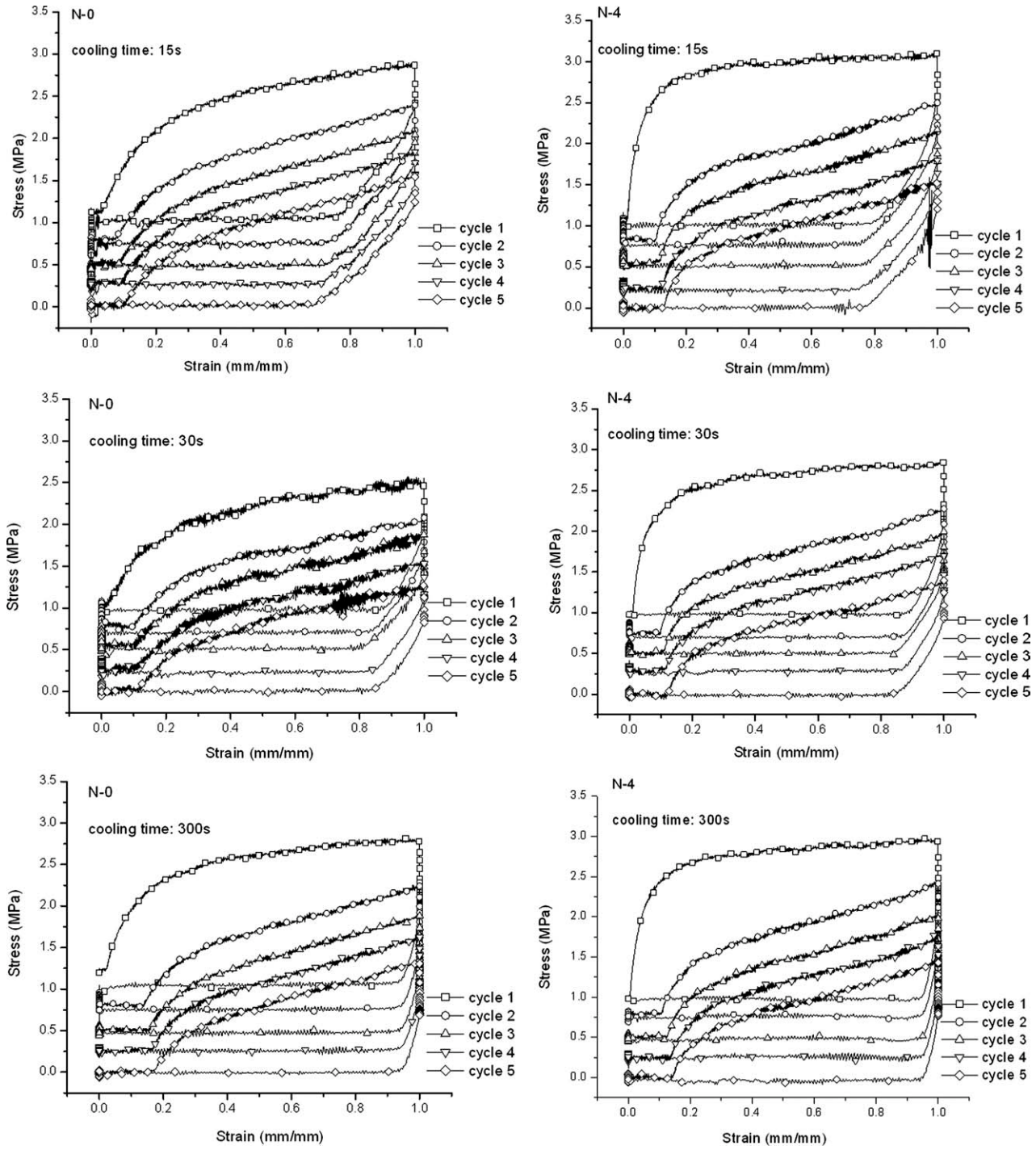

Figure 7 Cyclic tensile test (the maximum strain: 1 (mm/mm)) for *N*-0 and *N*-4 with various cooling time: 15, 30, 60, and 300 s, respectively. (Stress offset = (5-cycle number)*0.25 (MPa)).

segment phase), demonstrate the two-phase structures in all samples. DSC results also show the effect of CW on the crystallization of hard segment phase is not comparable with thermal history. Isothermal crystallization kinetic method was applied to analyze the effect of loading content of CW on crystallization of reversible phase at room temperature (16–32°C) after quenching from 75°C. It was found that the more CW filled in CW/SMPU, the higher the crystallization rate of reversible phase will be; the crystallization mechanism of reversible phase in SMPU is quite different from the pure SMPU, judging from the decreased n value from around 2.5 in pure SMPU (*N*-0) to 1.5–2.0 in the nano-composites; the main crystallization type of reversible phase through isothermal crystallization process is

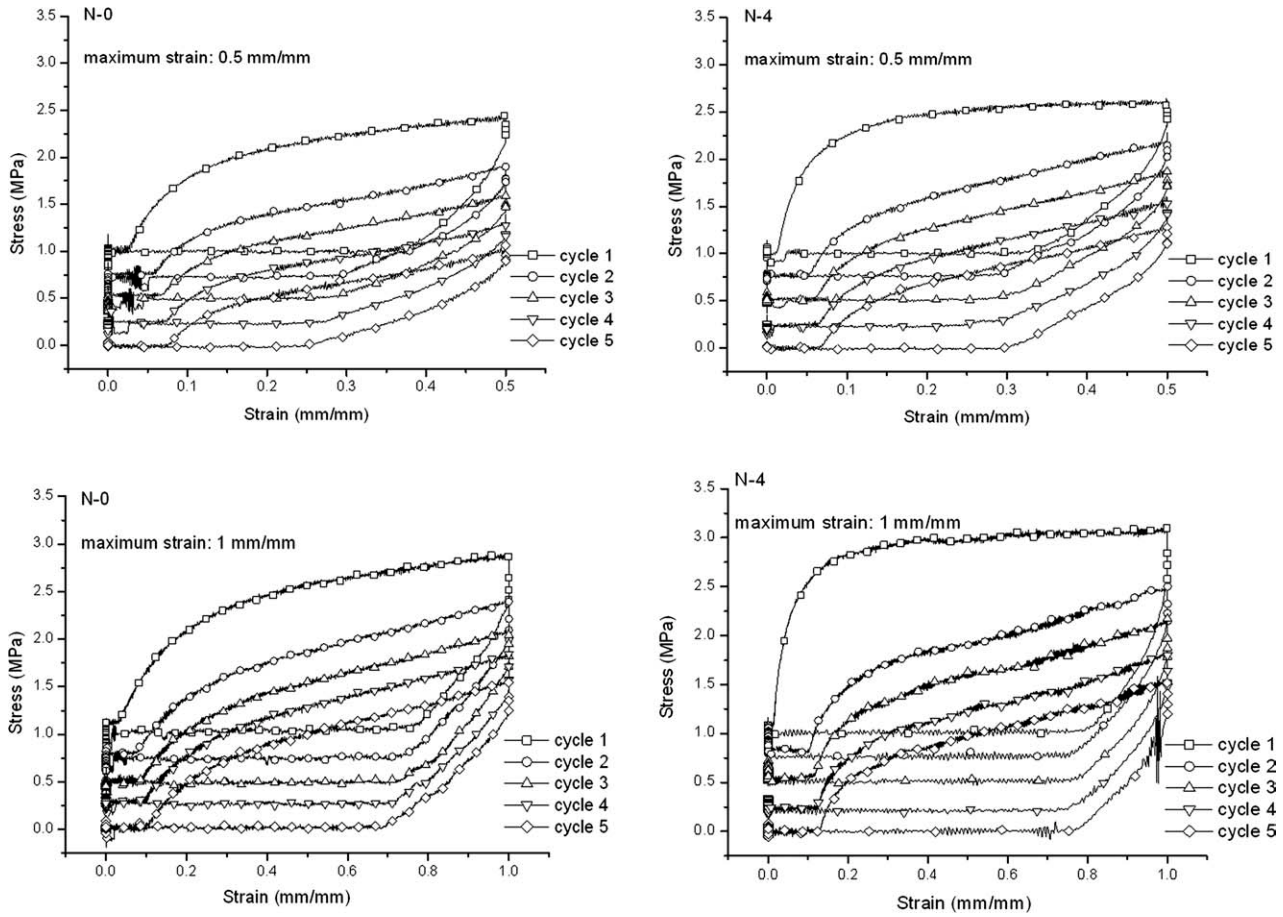

Figure 8 Cyclic tensile test (the cooling time: 15 s) for *N*-0 and *N*-4 with maximum strain: 0.5 and 1.0 mm/mm, respectively. (Stress offset = (5-cycle number)*0.25 (MPa)).

unchanged in all samples according to the XRD analysis. Besides, it was found the whole isothermal crystallization of this study in the temperature ranging from 16 to 32°C is dominated by nucleation term. For the crystallization rate, CW can greatly speed up the crystallization of reversible phase of SMPU. The excellent nucleation effect of cellulose whiskers for the reversible phase of SMPU leads to the drop of activity energy from 134.1 kJ/mol (*N*-0) to 95.1 kJ/mol (*N*-4), and accordingly decreases the influence of temperature on crystallization rate, so as to obtain the high crystallization rate in relative high temperature. Cyclic tensile tests illustrate the addition of CW content can engender rapid shape fixity ability after a relative short cooling time; the shape fixity ratio of nano-composites and the control sample after sufficient cooling all can be identically high.

This project was supported by the Hong Kong Research Grants Council project(RGC-GRF/518209), the Hong Kong ITF research project GHS/088/04,GHP/045/07TP,the Niche Area Fund of Hong Kong Polytechnic University (J-BB6M) and the Opening Project of State Key Laboratory of Polymer Materials Engineering (Sichuan University) (200803).

References

1. Lendlein, A.; Kelch, S. Angewandte Chemie-Int Ed 2002, 41, 2034.
2. Lendlein, A.; Langer, R. Science 2002, 296, 1673.
3. Li, F. K.; Zhang, X.; Hou, J. N.; Xu, M.; Luo, X. L.; Ma, D. Z.; Kim, B. K. J Appl Polym Sci 1997, 64, 1511.
4. Kim, B. K.; Shin, Y. J.; Cho, S. M.; Jeong, H. M. J Polym Sci: Part B: Polym Phys 2000, 38, 2652.
5. Jeong, H. M.; Lee, S. Y.; Kim, B. K. J Mater Sci 2000, 35, 1579.
6. Tobushi, H.; Hashimoto, T.; Ito, N.; Hayashi, S.; Yamada, E. J Intelligent Mater Syst Struct 1998, 9, 127.
7. Kim, B. K.; Lee, S. Y.; Lee, J. S.; Baek, S. H.; Choi, Y. J.; Lee, J. O.; Xu, M. Polymer 1998, 39, 2803.
8. Tobushi, H.; Hara, H.; Yamada, E.; Hayashi, S. Smart Mater Struct 1996, 5, 483.
9. Kim, B. K.; Lee, S. Y.; Xu, M. Polymer 1996, 37, 5781.
10. Hayashi, S.; Ishikawa, N. J Coated Fabrics 1993, 23, 74.
11. Hu, J. L.; Zeng, Y. M.; Yan, H. J. Text Res J 2003, 73, 172.
12. Hu, J. L.; Yang, Z. H.; Yeung, L. Y.; Ji, F. L.; Liu, Y. Q. Polym Int 2005, 54, 854.
13. Hu, J. L.; Ji, F. L.; Wong, Y. W. Polym Int 2005, 54, 600.
14. Zhu, Y.; Hu, J. L.; Yeung, K. W.; Fan, H. J.; Liu, Y. Q. Chinese J Polym Sci 2006, 24, 173.
15. Zhu, Y.; Hu, J. L.; Yeung, L. Y.; Liu, Y.; Ji, F. L.; Yeung, K. W. Smart Mater Struct 2006, 15, 1385.
16. Huang, W. M.; Yang, B.; An, L.; Li, C.; Chan, Y. S. Appl Phys Lett 2005, 86, 114105.

17. Cho, J. W.; Kim, J. W.; Jung, Y. C.; Goo, N. S. Macromol Rapid Commun 2005, 26, 412.
18. Chen, S. J.; Su, J. C.; Zhao, W. B.; Liu, P. S. Polym Mater Sci Eng 2005, 21, 166.
19. Cha, D. I.; Kim, H. Y.; Lee, K. H.; June, Y. C.; Cho, J. W.; Chun, B. C. J Appl Polym Sci 2005, 96, 460.
20. Li, F. K.; Zhang, X.; Hou, J. A.; Zhu, W.; Xu, M. Acta Polymerica Sinica 1996, 4, 462.
21. Hou, J. A.; Ma, X. Q.; Luo, X. L.; Ma, D. Z.; Zhang, X.; Zhu, W.; Xu, M. In The International Symposium on Polymer Alloys and Composites; Choy, C. L.; Shin, F. G., Eds.; Hong Kong Polytechnic University, Hong Kong Polytechnic University: Hong Kong, 1992; p 211.
22. Zhu, Y.; Hu, J.; Yeung, K.-W. Acta Biomaterialia 2009, 5, 3346.
23. Zhu, Y.; Hu, J.; Choi, K.-F.; Meng, Q.; Chen, S.; Yeung, K.-W. Polym Adv Technol 2008, 19, 328.
24. Marcovich, N. E.; Auad, M. L.; Bellesi, N. E.; Nutt, S. R.; Aranguren, M. I. J Mater Res 2006, 21, 870.
25. Helbert, W.; Cavaille, J. Y.; Dufresne, A. Polym Compos 1996, 17, 604.
26. Eichhorn, S. J.; Young, R. J. Cellulose 2001, 8, 197.
27. Dong, X. M.; Revol, J. F.; Gray, D. G. Cellulose 1998, 5, 19.
28. Oksman, K.; Mathew, A. P.; Bondeson, D.; Kvien, I. Compos Sci Technol 2006, 66, 2776.
29. Favier, V.; Canova, G. R.; Shrivastava, S. C.; Cavaille, J. Y. Polym Eng Sci 1997, 37, 1732.
30. Capadona, J. R.; Shanmuganathan, K.; Tyler, D. J.; Rowan, S. J.; Weder, C. Science 2008, 319, 1370.
31. Samir, M. A. S. A.; Alloin, F.; Sanchez, J. Y.; El Kissi, N.; Dufresne, A. Macromolecules 2004, 37, 1386.
32. Zhu, Y.; Hu, J. L.; Yeung, K. W.; Choi, K. F.; Liu, Y. Q.; Liem, H. M. J Appl Polym Sci 2007, 103, 545.
33. Dufresne, A.; Cavaille, J. Y.; Helbert, W. Polym Compos 1997, 18, 198.
34. Chen, H.-L.; Li, L.-J.; Ou-Yang, W.-C.; Hwang, J. C.; Wong, W.-Y. Macromolecules 1997, 30, 1718.
35. Brunette, C. M.; Hsu, S. L.; MacKnight, W. J. Macromolecules 1982, 15, 71.
36. Avrami, M. J Chem Phys 1939, 7, 1103.
37. Liu, S.; Yu, Y.; Cui, Y.; Zhang, H.; Mo, Z. J Appl Polym Sci 1998, 70, 2371.
38. Li, C.; Tian, G.; Zhang, Y.; Zhang, Y. Polym Test 2002, 21, 919.
39. Kim, S. H.; Ahn, S. H.; Hirai, T., Polymer 2003, 44, 5625.
40. Alwattari, A. A.; Lloyd, D. R. Polymer 1998, 39, 1129.
41. Lin, C. C. Polym Eng Sci 1983, 23, 113.
42. Cebe, P.; Hong, S.-D. Polymer 1986, 27, 1183.
43. Kuo, S. W.; Chan, S. C.; Chang, F. C. J Appl Polym Sci 2004, 42, 117.
44. Li, J.; Zhou, C. X.; Wang, G.; Tao, Y.; Liu, Q.; Li, Y. Polym Test 2002, 21, 583.
45. D Turnbull, J. F. J Chem Phys 1949, 17, 71.
46. Hoffman, J. D.; Weeks, J. J. J Chem Phys 1962, 37, 1723.
47. Liu, Y.; Pan, C. Eur Polym J 1998, 34, 621.
48. Bogdanow, B.; Toncheva, V.; Schacht, E.; Finelli, L.; Sarti, B.; Scandola, M. Polymer 1999, 40, 3171.
49. Alamo, R. G.; Viers, B. D.; Mandelkern, L. Macromolecules 1995, 28, 3205.
50. Alamo, R. G.; Chan, E. K. M.; Mandelkern, L. Macromolecules 1992, 25, 6381.
51. Jeong, H. M.; Ahn, B. K.; Kim, B. K. Polym Int 2000, 49, 1714.